Citation: Juan Garcia-Lechuz, Rosario Aragues, and Gonzalo Lopez-Nicolas. Distributed quadratic-shape formation control. IEEE Transactions on Industrial Electronics, pages 1-12, 2026

Distributed Quadratic-Shape Formation Control

Juan García-Lechuz, Rosario Aragüés, *Senior Member, IEEE*, and Gonzalo López-Nicolás, *Senior Member, IEEE*

***Abstract*—This article presents a distributed method to perform multiagent formation control and maneuvering while allowing for linear and quadratic deformations of the robotic formation relative to a target configuration in 2-D. First, a novel convex-optimization-based gain matrix design for the control law is proposed. Then, by exploiting the properties of stress matrices with specific kernel constraints, our leader–follower strategy enables the set of agents to adopt quadratic deformations in the plane, e.g., bending, while maintaining sufficient resemblance to the reference formation. We provide a stability analysis of the proposed formation control and experiments to demonstrate the theoretical results.**

***Index Terms*—Distributed algorithms, formation control, multiagent systems, networked control systems, robotics.**

I. Introduction

THE formation control and maneuvering of mobile multiagent systems can be addressed via various strategies, with various applications such as manipulation and object transport [1]. To this end, distributed approaches, where the control actions depend linearly on interagents' relative positions, ensure higher scalability, less expensive computations, and robustness to uncertainty [2], [3], [4].

When the formation must also move along complex trajectories, new challenges arise. Some methods allow for modifying the size of a target formation [5] or even the relative angles between nodes of the target formation [6]. Although these methods allow for complex maneuvers and traversing narrow corridors, they have difficulty describing curves and dynamically reorienting the team. In this context, our work presents a distributed leader–follower approach to perform formation control of a team of agents, not only converging to a target formation, but also allowing the agents to describe quadratic deformations of this same target. As an example, a method that allows for such flexibility in maneuvering can be used in the collaborative transport of deformable objects along constrained and curved corridors. In this case, the agents need to dynamically modify their orientation to adapt to the curve, taking advantage of the deformability of the object.

A. Related Work

The multiagent team is defined by an interagent sensing static graph and single-integrator dynamics, which allows the control law to be expressed via a constant Laplacian-like matrix. The work of Wang et al. [7] studied the relation between the complex Laplacian matrix and the agents' graph connectivity, designing a 2-D coordinate-free formation control approach, based solely on relative distance measurements and allowing scale and rotation reconfigurations. A systematic construction method of the Laplacian matrix was later developed by Lin et al. [4]. Another technique to compute a gain Laplacian-like matrix was proposed by Fathian et al. [8], considering block matrix constraints and optimized using semidefinite programming (SDP). They also demonstrated its transferability to agents with other dynamic models [9]. A problem arising from this type of method is the need to control the degrees of freedom, that is, scaling and orientation, to improve its transferability to real-world applications. In Lin et al. [10], the desired rotation and scale were determined through a small set of leaders, making leader–follower coordination a natural mechanism for formation specification and maneuvering. It is worth noting that coordinate-free formation control can also be achieved through angle-based control strategies [11], which can lead to more efficient communication. However, angle-based methods are also restricted to rotation and scale reconfigurations. Another approach combining generalized Laplacian matrices and a leader–follower strategy was presented by Zhao [6]. This work addressed the formation control of a team of agents with dynamics, allowing the reconfiguration of the agents to affine transformations of the target formation. More recent works, such as [12], have expanded the leader–follower strategy to consensus-tracking problems in heterogeneous multiagent systems, where distributed protocols are designed so that agents track a moving target or reference trajectory through local interactions. Formation maneuvering for heterogeneous teams was also tackled by Wang et al. [13] using the Laplacian-based method. Later, Su et al. [14] used time-varying convex optimization to better address complex obstacle avoidance problems. The rotation and maneuvering problem was also tackled by Aranda et al. [3] with a Laplacian-based approach combining translation,

Received 22 December 2025; revised 25 March 2026 and 30 April 2026; accepted 29 May 2026. This work was supported in part by the project REMAIN - S1/1.1/E0111 (Interreg Sudoe Programme, ERDF), in part by the project PID2021-124137OB-I00 and project PID2024-159279OB-I00 funded by MICIU/AEI/10.13039/501100011033 and ERDF/EU, and in part by PRE2022-10422. *(Corresponding author: Juan García-Lechuz.)*

The authors are with the Instituto de Investigación en Ingeniería de Aragón (I3A), Universidad de Zaragoza, 50018 Zaragoza, Spain (e-mail: jgarcialechuz@unizar.es; raragues@unizar.es; gonlopez@unizar.es).

This article has supplementary downloadable material available at https://doi.org/10.1109/TIE.2026.3702186, provided by the authors.

Digital Object Identifier 10.1109/TIE.2026.3702186

© 2026 The Authors. This work is licensed under a Creative Commons Attribution 4.0 License. For more information, see https://creativecommons.org/licenses/by/4.0/

This article has been accepted for inclusion in a future issue of this journal. Content is final as presented, with the exception of pagination.

shape-preserving, and affine transformations of a reference configuration. However, as already stated, these types of formations are less adaptable than complex curved formations.

In another contribution, Aranda et al. [15] addressed the control of curved formations parameterizing closed curves with low-frequency Fourier descriptors. Based on a similar parametrization, Zhang et al. [16] developed a leader–follower controller to form open and closed curves with nonholonomic agents. Although both works provide formation with great flexibility, they do not specifically consider maneuvers in which the formation needs to bend. This was considered by Marcos-Saavedra et al. [17]. They designed a centralized control capable of allowing linear and quadratic deformations of the formation relative to the target configuration. They considered deformation modes, already studied for shape control [18], to preserve the integrity of a deformable object while increasing transport flexibility by bending the formation. The problem of deformable object transport was also addressed by Herguedas et al. [19] using a centralized approach, and by Alonso-Mora et al. [20], taking advantage of the object's properties to avoid obstacles.

B. Challenges and Contribution

Extending the Laplacian-based control frameworks to nonrigid quadratic deformations presents several key design challenges. First, we aim to achieve extra maneuverability while maintaining a distributed coordinate-free method. This makes gains design nontrivial. Second, the space of admissible formations must be a nonrigid quadratic subspace, with more degrees of freedom than in the rigid or affine case. Thus, it is crucial to control convergence to a specific deformation within the considered space. Finally, the proposed method must ensure stability and avoid unwanted deformations.

Motivated by the aforementioned, this work presents a distributed method to perform multirobot formation control while allowing the agents to form linear and quadratic deformations of the target configuration. The main contributions are:

1) Based on the SDP approach for convex optimization [8], we propose a novel offline gain design of a complex-Laplacian-like matrix, including second-order deformation modes in the formation to which agents converge. This design leads to the formation control of more complex nonrigid formations, beyond scaling or rotations. In addition, the online control computation relies on local relative position measurements of the surrounding neighbors, without requiring a global coordinate frame.
2) We propose a leader–follower strategy to restrict convergence to a particular shape formation and deal with dynamic leaders traversing complex trajectories with curves. This leader–follower strategy, combined with the gain matrix design, allows the agents to maneuver by bending the formation.
3) We demonstrate that quadratic deformations are stably realizable using the proposed method, and include simulations and experiments.

Compared to other formation control methods such as [5], our method is not restricted to regular polygon formations, but instead, allows convergence to any nondegenerate reference formation in 2-D. Furthermore, compared to other coordinate-free methods such as [11], or complex-Laplacian-based methods such as [7], [21], or [8], our method is not restricted to rescaling and reorientation of a reference formation. Rather, it allows convergence to a nonrigid quadratic deformation space, extending the applicability of the complex-Laplacian matrix. On the other hand, affine formation control methods such as [3], [6] are restricted to affine transformations of the reference formation. Compared to affine block-Laplacian-based methods such as [6], using a complex-Laplacian matrix can lead to higher maneuverability [22]. By using leading agents, our method allows maneuvers not limited to affine transformations, as in [6], [13], [14], but including quadratic transformations that bend the formation in an organized manner. Methods presented in [15] and [16] rely on explicit curve representations and assume that the curve itself is the control objective. In contrast, our method does not require estimating or maintaining a curve model. It also does not require predesigning the desired formation as in [17]. Our method allows the formation to evolve within the considered deformations guided by the leaders, without any gains recalculations. In addition, [15], [16], [17] are centralized, which limits their scalability.

The rest of this article is organized as follows. In Section II-A, the quadratic formation control problem is formulated. In Section II-B, the distributed and coordinate-free control law is presented. In Section II-C, the realizability and stability of the proposed quadratic-shape formation control are demonstrated. In Section II-D, a gain matrix design is proposed. Then, Section II-E, presents the method for maneuvering by following and tracking a set of leaders. Sections III and IV contain the simulations and experimental results to evaluate the proposed approach. Finally, the conclusions of this article are summarized in Section V.

II. Distributed Quadratic Formation Control

A. Problem Statement

We consider a team of $n \in \mathbb{N}$ agents with their states as positions in $\mathbb{R}^2$, with the interagent sensing topology described by an undirected graph $\mathcal{G} = (\mathcal{V}, \mathcal{E})$, where $\mathcal{V} = \mathbb{N}_n = \{1, 2, \ldots, n\}$ is the set of vertices, and $\mathcal{E} \subset \mathcal{V} \times \mathcal{V}$ is the set of edges. Let us also consider that graph $\mathcal{G}$ is four-rooted, which imposes that $n \geq 4$. Each vertex of the graph represents an agent, and an edge from vertex $i \in \mathcal{V}$ to $j \in \mathcal{V}$ indicates that agents i and j are neighbors and they can measure their relative positions in their local coordinate frames. The set of neighbors of agent i is denoted by $\mathcal{N}_i = \{j \in \mathcal{V} | (i, j) \in \mathcal{E}\}$. On the other hand, the state of the formation in global coordinates is defined by the column vector $q = [q_1^\top, q_2^\top, \ldots, q_n^\top]^\top \in \mathbb{R}^{2n}$, being $q_i \in \mathbb{R}^2$ the state of agent i. Then, ${}^i q_j = R_i^{-1}(q_j - q_i)$ is the relative state of the neighbor $j \in \mathcal{N}_i$ in agents' i reference frame, being $R_i \in SO(2)$ the rotation matrix of the local coordinate frame of agent i with respect to the global coordinate frame. It is

This article has been accepted for inclusion in a future issue of this journal. Content is final as presented, with the exception of pagination.

considered that $q_i \neq q_j$ for $i \neq j$. Each agent is governed by single integrator dynamics, expressed as follows:

$$ {}^i\dot{q}_i = {}^iu_i \tag{1}$$

where ${}^iu_i \in \mathbb{R}^2$ represents the control input of agent i in its local coordinate frame. Let us consider a target formation $q^* = [q_1^{*\top}, q_2^{*\top}, \ldots, q_n^{*\top}]^\top \in \mathbb{R}^{2n}$ in global coordinates, which is considered to be not degenerated, being $q_i^* \in \mathbb{R}^2$ the state of agent i in the target formation. Let us also consider $q^\infty = [q_1^{\infty\top}, q_2^{\infty\top}, \ldots, q_n^{\infty\top}]^\top \in \mathbb{R}^{2n}$ the formation obtained at the convergence of the control in global coordinates.

We propose the following quadratic deformation of the target configuration q^*, defined as:

$$\mathcal{Q}(q^*) = (I_n \otimes L_1)q^* + (I_n \otimes L_2)q^*_{xx} + (I_n \otimes L_3)q^*_{xy} + (1_n \otimes h) \tag{2}$$

where $h \in \mathbb{R}^2$ is a translation vector, 1_n is the all-ones column vector of size n, $I_n \in \mathbb{R}^{n\times n}$ denotes the identity matrix, the symbol $\otimes$ is the Kronecker product and $L_1, L_2, L_3 \in \mathbb{R}^{2\times 2}$ are coefficient matrices of the form

$$L_l = \begin{bmatrix} c_l & -d_l \\ d_l & c_l \end{bmatrix} \quad l = 1, 2, 3 \tag{3}$$

being c_l and d_l scalar values. This reduces vectors in $\mathcal{Q}(q^*)$ to rotations and uniform scalings of the pure quadratic terms q^*_{xx}, the mixed terms q^*_{xy} and the linear components of q^*, which are defined as follows:

$$\begin{aligned} q^*_{xx} &= q^* \odot q^* \in \mathbb{R}^{2n}, \\ q^*_{xy} &= q^* \odot \left(I_n \otimes \begin{bmatrix} 0 & 1 \\ 1 & 0 \end{bmatrix} \right) q^* \in \mathbb{R}^{2n} \end{aligned} \tag{4}$$

where symbol $\odot$ denotes the Hadamard product. Hence, (2) defines a polynomial deformation of, at most, second-degree, applied to every agent in the reference formation. Fig. 1 illustrates the effect of each of the terms in (2) for a reference formation where the agents are horizontally aligned, see Fig. 1(a). Fig. 1(d) and (f) shows how the deformation in (2), evaluated in collinear agents, becomes a common parabolic function.

Remark 1: From (4), the contribution of the quadratic terms q^*_{xx} and q^*_{xy} in (2) depends strongly on the chosen origin and physical size of the formation. Thus, centering and rescaling (e.g., to unit size) the formation may be used to enhance the interpretability of $\mathcal{Q}(q^*)$.

If the state of every agent in q belongs to $\mathcal{Q}(q^*)$, the n agents form a quadratic deformation of q^*. Thereby, the control law that enables the state q of a group of agents to converge to a formation in the space $\mathcal{Q}(q^*)$ will be studied in this article.

B. Control Law

In order for a multiagent system to achieve a stable quadratic deformation of a target configuration in 2-D, we build up from the following strategy, studied by Fathian et al. [8] for formations under different types of transformation:

$$ {}^iu_i = \sum_{j\in\mathcal{N}_i} A_{ij}\, {}^iq_j \tag{5}$$

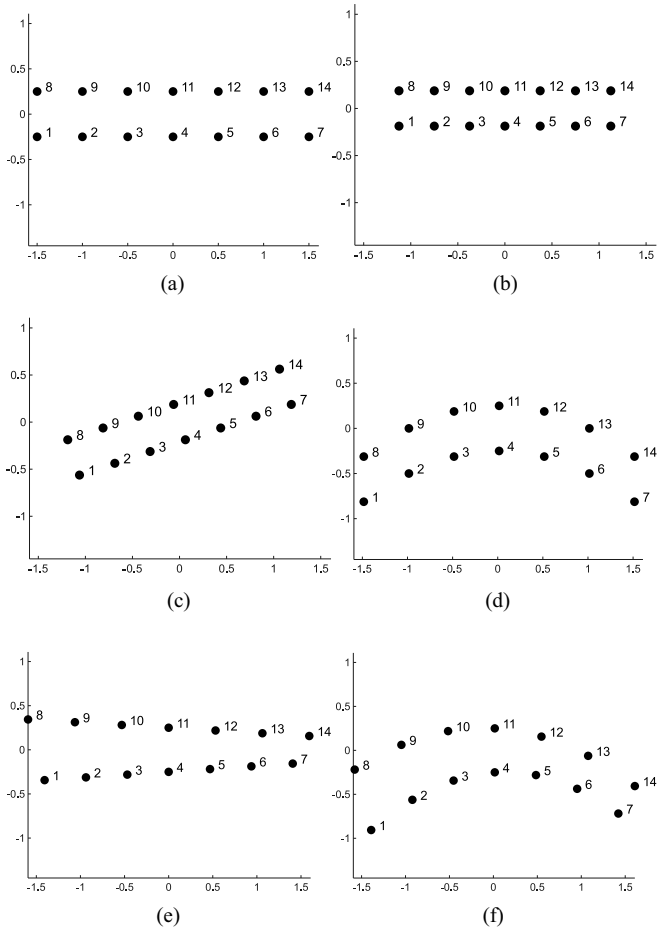


Fig. 1. Examples of quadratic deformations in $\mathcal{Q}(q^*)$. All terms of matrices L_1, L_2, L_3 are 0, except those specified in the footnote of each subfigure. (a) Reference ($c_1 = 1$). (b) Scale reduction ($c_1 = 0.75$). (c) Rotation and scaling ($c_1 = 0.75$, $d_1 = 0.25$). (d) Pure quadratic transformation ($c_1 = 1$, $d_2 = 0.25$). (e) Transformation based on mixed terms ($c_1 = 1$, $d_3 = 0.25$). (f) Quadratic transformation ($c_1 = 1$, $d_2 = 0.25$, $d_3 = 0.25$).

where $A_{ij} \in \mathbb{R}^{2\times 2}$ are constant control gain matrices designed and provided to agents in advance. An important consideration when designing matrices A_{ij} is that they must be compatible with a coordinate-free control. The following lemma establishes a structural condition to ensure this feature.

Lemma 1 (Coordinate-free control law [8]): Under control law (5), if the matrices A_{ij} and R_i commute, i.e., if $R_iA_{ij} = A_{ij}R_i$, then the closed-loop dynamics of the agents in global coordinates can be expressed as follows:

$$\dot{q} = Aq \tag{6}$$

in which $A = [A_{ij}] \in \mathbb{R}^{2n\times 2n}$, with $A_{ii} = -\sum_{j\in\mathcal{N}_i} A_{ij}$, and $A_{ij} = 0_{2\times 2}$ (the all-zeros matrix of size 2×2) for $j \notin \mathcal{N}_i$, meaning the agents are not neighbors.

Proof: From (1) and (5), dynamics in the global coordinate frame is as follows:

$$\begin{aligned} \dot{q}_i &= R_i\, {}^i\dot{q}_i \\ &= \sum_{j\in\mathcal{N}_i} R_iA_{ij}\, {}^iq_j = \sum_{j\in\mathcal{N}_i} R_iA_{ij}R_i^{-1}(q_j - q_i). \end{aligned} \tag{7}$$

This article has been accepted for inclusion in a future issue of this journal. Content is final as presented, with the exception of pagination.

From this, if the rotation and gain matrices commute, the control becomes independent of the local coordinate frame orientations, resulting in the global dynamics defined in (6)

$$\dot{q}_i = \sum_{j\in\mathcal{N}_i} A_{ij}R_iR_i^{-1}(q_j - q_i) = \sum_{j\in\mathcal{N}_i} A_{ij}(q_j - q_i). \quad (8)$$

□

Let us define A_{ij} as follows:

$$A_{ij} = \begin{bmatrix} a_{ij} & -b_{ij} \\ b_{ij} & a_{ij} \end{bmatrix} \quad (9)$$

where a_{ij} and b_{ij} are scalar gain values. This specific matrix structure is equivalent to the use of a complex Laplacian matrix [7], [21] and allows submatrices A_{ij} and R_i to commute. From this property, it follows that the closed-loop dynamics is invariant to the reference frame and does not require global information to converge.

C. Stabilization to a Quadratic Deformation

This section presents the properties of matrix A allowing a team of agents to converge asymptotically to $\mathcal{Q}(q^*)$ (2). We first state the conditions for stable quadratic deformation control on the proposed distributed setup (Theorem 1). Then, we analyze the required interagent connectivity (Theorem 2).

Theorem 1 (realizability and stability): Consider a team of n single integrator agents ($n \geq 4$) with closed-loop dynamics (6), and a four-rooted underlying communication topology. Consider also vectors 1_x and 1_y, which are defined as follows:

$$\begin{aligned} 1_x &= (1_n \otimes e_x) \in \mathbb{R}^{2n} \\ 1_y &= (1_n \otimes e_y) \in \mathbb{R}^{2n} \end{aligned} \quad (10)$$

where $e_x = [1, 0]^\top$ and $e_y = [0, 1]^\top$. If $A = [A_{ij}] \in \mathbb{R}^{2\times 2}$ is as in (9) and satisfies the following conditions:

$$A1_x = 0_{2n},\ A1_y = 0_{2n} \quad (11)$$

$$Aq^* = 0_{2n},\ Aq^*_{xx} = 0_{2n},\ Aq^*_{xy} = 0_{2n} \quad (12)$$

$$\lambda_i(A) \leq 0, \quad \forall i = 1, 2, \ldots, 2n \quad (13)$$

where 0_{2n} is the all-zeros column vector of size $2n$ and $\lambda_i(A)$ is an eigenvalue of a matrix A, with i the index of the eigenvalue in the spectrum of the matrix. Then, under the distributed local control law (5), starting from any initial configuration q, the agents converge asymptotically to a quadratic deformation in $\mathcal{Q}(q^*)$ (2) involving uniform rotations and scalings of the pure quadratic terms q^*_{xx}, the mixed terms q^*_{xy} and the linear components of q^*.

Proof: Following (9), we can decompose matrix A in the following Kronecker product:

$$A = M_a \otimes I_2 + M_b \otimes J \quad (14)$$

being $M_a = [a_{ij}] \in \mathbb{R}^{n\times n}$, $M_b = [b_{ij}] \in \mathbb{R}^{n\times n}$, $I_2 \in \mathbb{R}^{2\times 2}$ the identity matrix and

$$J = \begin{bmatrix} 0 & -1 \\ 1 & 0 \end{bmatrix}.$$

Then, applying the mixed-product property of the Kronecker product to condition (11), we obtain

$$\begin{aligned} A(1_n \otimes e_x) &= (M_a \otimes I_2 + M_b \otimes J)(1_n \otimes e_x) \\ &= (M_a 1_n) \otimes (I_2 e_x) + (M_b 1_n) \otimes (J e_x) \\ &= (M_a 1_n) \otimes e_x + (M_b 1_n) \otimes e_y = 0_{2n} \\ A(1_n \otimes e_y) &= (M_a \otimes I_2 + M_b \otimes J)(1_n \otimes e_y) \\ &= (M_a 1_n) \otimes (I_2 e_y) + (M_b 1_n) \otimes (J e_y) \\ &= (M_a 1_n) \otimes e_y - (M_b 1_n) \otimes e_x = 0_{2n}. \end{aligned} \quad (15)$$

Since e_x and e_y are linearly independent, the following equations hold:

$$\begin{aligned} M_a 1_n &= 0_n \\ M_b 1_n &= 0_n. \end{aligned} \quad (16)$$

Consequently, we can apply the mixed-product property of the Kronecker product to the matrix multiplication of A and the translational component of (2) as follows:

$$\begin{aligned} A(1_n \otimes h) &= (M_a \otimes I_2 + M_b \otimes J)(1_n \otimes h) \\ &= (M_a 1_n) \otimes h + (M_b 1_n) \otimes (Jh) = 0_{2n} \end{aligned} \quad (17)$$

which means that any uniform translation h of the agents, as in (2), belongs to the null space of A.

On the other hand, from condition (12), we can deduce that the quadratic transformation resulting from applying matrices L_1, L_2 and L_3 as in (2) belongs to the $\ker(A)$ if matrices $(I_n \otimes L_l)$, $l = 1, 2, 3$, commute with A

$$\begin{aligned} &A((I_n \otimes L_1)q^* + (I_n \otimes L_2)q^*_{xx} + (I_n \otimes L_3)q^*_{xy}) \\ &= A(I_n \otimes L_1)q^* + A(I_n \otimes L_2)q^*_{xx} + A(I_n \otimes L_3)q^*_{xy} \\ &= (I_n \otimes L_1)Aq^* + (I_n \otimes L_2)Aq^*_{xx} + (I_n \otimes L_3)Aq^*_{xy} = 0_{2n}. \end{aligned} \quad (18)$$

Again, using the mixed-product property of the Kronecker product, we can develop the following expressions for $l = 1, 2, 3$:

$$\begin{aligned} A(I_n \otimes L_l) &= (M_a \otimes I_2 + M_b \otimes J)(I_n \otimes L_l) \\ &= (M_a I_n) \otimes (I_2 L_l) + (M_b I_n) \otimes (J L_l) \\ &= M_a \otimes L_l + M_b \otimes (J L_l) \\ (I_n \otimes L_l)A &= (I_n \otimes L_l)(M_a \otimes I_2 + M_b \otimes J) \\ &= (I_n M_a) \otimes (L_l I_2) + (I_n M_b) \otimes (L_l J) \\ &= M_a \otimes L_l + M_b \otimes (L_l J). \end{aligned} \quad (19)$$

Then, taking into account (3), L_l and J commute, and we can write

$$(I_n \otimes L_l)A = M_a \otimes L_l + M_b \otimes (JL_l) = A(I_n \otimes L_l) \quad (20)$$

proving that the matrix A commutes with $(I_n \otimes L_l)$, $l = 1, 2, 3$. Therefore, any vector in $\mathcal{Q}(q^*)$ (2) belongs to $\ker(A)$. Breaking down (2), the term of translations $(1_n \otimes h)$ adds two degrees of freedom to the $\ker(A)$, one for each spatial axis, as well as the rotation and uniform scaling of each of the three remaining terms. This results in at least eight degrees of freedom for $\ker(A)$. Moreover, as it is demonstrated below, given that the

This article has been accepted for inclusion in a future issue of this journal. Content is final as presented, with the exception of pagination.

underlying communication topology is four-rooted, the rank of A is as follows:

$$\begin{aligned}\dim(\ker(\mathrm{A})) &= 8\\ \operatorname{rank}(A) &= 2n-8.\end{aligned} \tag{21}$$

To generalize, we now consider a nonsymmetrical diagonalizable gain matrix. Let us define $V=[v_1,v_2,\ldots,v_{2n}]\in\mathbb{R}^{2n\times 2n}$ and $W=[w_1,w_2,\ldots,w_{2n}]\in\mathbb{R}^{2n\times 2n}$ as the matrices whose columns are the right and left eigenvectors of A, respectively. If we consider the dynamics of the system in (6), we can define the evolution of the agents' state $q(t)$ as a function of time t

$$\begin{aligned}q(t) &= e^{At}q(0)=Ve^{\Lambda t}V^{-1}V\alpha=Ve^{\Lambda t}\alpha\\ &= \alpha_1 e^{\lambda_1(A)t}v_1+\alpha_2 e^{\lambda_2(A)t}v_2+\ldots+\alpha_{2n}e^{\lambda_{2n}(A)t}v_{2n}\end{aligned} \tag{22}$$

where Λ is the diagonal eigenvalue matrix of A, and $\alpha=[\alpha_1,\alpha_2,\ldots,\alpha_{2n}]^\top\in\mathbb{R}^{2n}$ is the column vector of coefficients that decomposes $q(0)$ as a linear combination of the eigenvectors in V. These coefficients can be calculated using the dual basis involving the left and the right eigenvectors, such that

$$\alpha_i=\frac{w_i^\top q(0)}{w_i^\top v_i}i=1,2,\ldots,2n. \tag{23}$$

If A is such that (13) is satisfied, and considering $\mathcal{I}=\{i\mid\lambda_i(A)=0\}$, the following equation is also true:

$$q^\infty=\lim_{t\to\infty}q(t)=\sum_{i\in\mathcal{I}}\alpha_i v_i=V_{\mathcal{I}}\alpha_{\mathcal{I}} \tag{24}$$

where $V_{\mathcal{I}}\in\mathbb{R}^{2n\times 8}$ denotes the matrix of right eigenvectors forming a basis of $\ker(A)$, and $\alpha_{\mathcal{I}}\in\mathbb{R}^8$ the vector of coefficients in α corresponding to indices in subset $\mathcal{I}$. Thus, we can develop (24) and (23) in the following expression for the convergence of $q(t)$:

$$q^\infty=\lim_{t\to\infty}q(t)=V_{\mathcal{I}}\alpha_{\mathcal{I}},=V_{\mathcal{I}}(W_{\mathcal{I}}^\top V_{\mathcal{I}})^{-1}W_{\mathcal{I}}^\top q(0) \tag{25}$$

where $W_{\mathcal{I}}\in\mathbb{R}^{2n\times 8}$ is the matrix of left eigenvectors forming a basis of $\ker(A)$. This means that under conditions (11) to (13), agents converge asymptotically to a projection of $q(0)$ onto $\ker(A)$, i.e., a vector in $\mathcal{Q}(q^*)$ (2), which is an asymptotically stable set. □

In contrast to the affine formation control in [6], the proposed gain matrix excludes nonsimilar linear transformations from $\ker(A)$. It avoids nondesired quadratic deformations and, from (18), ensures that (3) and (9) commute and deformations are realizable under the distributed coordinate-free control (5).

An important consideration in Theorem 1 is that the underlying graph is four-rooted, meaning that the motion of each agent is determined by the motion of four root agents. This requirement establishes the minimum connectivity required to converge to a quadratic deformation in $\mathcal{Q}(q^*)$, and is stated in the following theorem.

Theorem 2 (four-rooted connectivity): Consider a team of n single integrator agents ($n\geq 4$) with closed-loop dynamics (6) and interagent topology described by graph $\mathcal{G}$. If A is as in (9) and satisfies conditions in Theorem 1. Then, $\operatorname{rank}(A)=2n-8$, if and only if $\mathcal{G}$ is four-rooted.

Proof: This theorem can be proved using the proof of Theorem 3.2 in [21]. Suppose that the graph $\mathcal{G}$ is not four-rooted, i.e., we cannot find four nodes to be roots from which all the nodes are four-reachable [21]. Considering (21), there must be eight rows of A which can be transformed to 0_{2n} vectors by elementary row operations. Choose the four nodes corresponding to the eight rows as roots, and after removing up to three nodes, some nodes are not reachable from the subset of roots. Suppose after removing a set of three nodes, there exists a subset W consisting of $w-1$ nodes which are not reachable from any root and a set $\bar{W}$ consisting of $n-(w+2)$ nodes which are reachable from one of the roots. Relabel the nodes in W as $1,\ldots,w-1$ and relabel the nodes in $\bar{W}$ as $w+3,\ldots,n$. Then it is certain that the nodes in W are not reachable from any node in $\bar{W}$. Equivalently, $A_{ij}=0_{2\times 2}$ for $i\in W$ and $j\in\bar{W}$. Thus A is of the following form:

$$\begin{bmatrix}A_w & C_w & 0_{2(w-1)\times 2(n-(w+2))}\\ * & * & *\end{bmatrix} \tag{26}$$

where $A_w\in\mathbb{R}^{2(w-1)\times 2(w-1)}$ and $C_w\in\mathbb{R}^{2(w-1)\times 6}$. Considering two of the eigenvectors in Theorem 1

$$\begin{aligned}[A_w\ C_w\ 0_{2(w-1)\times 2(n-(w+2))}]\,1_x&=0\\ [A_w\ C_w\ 0_{2(w-1)\times 2(n-(w+2))}]\,1_y&=0.\end{aligned} \tag{27}$$

As 1_x and 1_y are linearly independent by assumption, then $\operatorname{rank}([A_w\ C_w])\leq 2w-3$, which means that there exists at least a row that can be turned into a zero vector under elementary row operations. Therefore, $\operatorname{rank}(A)<2n-8$. □

Note that if the considered graph is not four-rooted, then $\dim(\ker(A))$ can exceed 8. In that case, the controller may converge to unintended formations within an enlarged invariant space, and the global guarantees of convergence to $\mathcal{Q}(q^*)$ no longer hold.

D. Gain Design via Optimization

Our approach for computing the gain matrix A (6) is based on the semidefinite programming (SDP) method first proposed by Lin et al. [4] and extended by Fathian et al. [2] to meet other kernel conditions.

Considering the definitions given in (4), let $N=[q^*,q^*_{xx},q^*_{xy},1_x,1_y]\in\mathbb{R}^{2n\times 5}$ to be the desired vectors in the kernel of matrix A, to fulfill conditions (11) and (12) stated in Theorem 1. Using the singular value decomposition of N, i.e. $N=\mathrm{USV}^\top$, we can define an orthonormal basis $Q\in\mathbb{R}^{2n\times(2n-5)}$ of the orthogonal complement of the image of N. This basis is computed as the last $2n-5$ columns of matrix $U\in\mathbb{R}^{2n\times 2n}$. From the projection of A into the computed orthonormal basis, $Q^\top AQ$, we can compute the nonimposed eigenvalues of the matrix A, which are different from zero. Then, a stability matrix that fulfills conditions (11)

This article has been accepted for inclusion in a future issue of this journal. Content is final as presented, with the exception of pagination.

Algorithm 1: Gain Matrix Design.

Input: $\mathcal{G}$, $q^* \in \mathbb{R}^{2n}$.
Output: Gain matrix $A \in \mathbb{R}^{2n\times 2n}$.

Step 1: Compute q^*_{xx} and q^*_{xy} as in (4).
Step 2: Define $N = [q^*, q^*_{xx}, q^*_{xy}, 1_x, 1_y] \in \mathbb{R}^{2n\times 5}$.
Step 3: Compute SVD of $N = USV^\top$.
Step 4: Define Q as the last $2n-5$ columns of matrix U.
Step 5: Compute A by solving (28).

to (13) can be computed by solving the following convex optimization problem:

$$
\begin{aligned}
A = \underset{a_{ij},b_{ij}}{\operatorname{argmin}} & (\lambda_{\max}(Q^\top A Q)) \\
& \text{Subject to} \\
& A = A^\top \\
& A\,N = 0_{2n\times 5} \\
& \lambda_{\max}(Q^\top A Q) \le 0 \\
& \begin{bmatrix} A_{2i-1,\,2j-1} & A_{2i-1,\,2j} \\ A_{2i,\,2j-1} & A_{2i,\,2j} \end{bmatrix} = \begin{cases} \begin{bmatrix} a_{ij} & -b_{ij} \\ b_{ij} & a_{ij} \end{bmatrix}, \forall (i,j) \in \mathcal{E}. \\ 0_{2\times 2},\ \forall (i,j) \notin \mathcal{E}. \end{cases}
\end{aligned} \tag{28}
$$

being $\lambda_{\max}(\cdot)$ the eigenvalue of a matrix with the largest real part. The objective in (28) minimizes the maximum nonzero eigenvalue of A, making it as negative as possible. Thus, it minimizes the slowest convergence rate of the formation error dynamics, thereby accelerating the system's convergence. On the other hand, the optimization constraints impose an undirected graph and ensure that matrix A fulfills the conditions in Theorem 1 and (9), and adjusts to the connectivity of the sensing topology $\mathcal{E}$. The proposed offline gain design has been summarized in Algorithm 1.

It should be emphasized that the gain matrix is obtained once through offline centralized optimization, but the execution of the control is fully distributed once each agent knows the optimized gain matrix.

Remark 2: From (2) and (25), it can be deduced that the particular transformation in $\mathcal{Q}(q^*)$ to which the control converges depends on agents' initial states. Therefore, any deformation in $\mathcal{Q}(q^*)$ can be achieved without recomputing gains.

E. Leader Following and Tracking

As stated in Remark 2, under control law (6), the team of agents converge to a configuration in $\mathcal{Q}(q^*)$ which is not unique, and depends on the initial configuration $q(0)$ and the deformation modes composing $\ker(A)$, with eight degrees of freedom (21). The following lemma outlines a way to restrict the solution to a desired deformation.

Lemma 2 (Unique deformation via leader selection): Consider a team of n single integrator agents ($n \ge 4$) with closed-loop dynamics (6), and a 4-rooted underlying communication topology. Let A be a block-Laplacian that fulfills conditions in Theorem 1. If four agents (leaders) are anchored to noncollinear fixed positions, then there exists a unique configuration $q^\infty \in \mathcal{Q}(q^*)$ satisfying the leader constraints. Hence, the closed-loop system converges asymptotically to this unique solution from any initial configuration of the remaining $n-4$ followers.

Proof: Anchoring a single agent in 2-D-space imposes two independent linear constraints on q_∞. Anchoring four agents to prescribed noncollinear positions imposes 8 independent linear constraints that eliminate the eight degrees of freedom of $\ker(A)$. Consequently, the closed-loop system asymptotically converges to the same rigid solution independently of the initial configuration of the remaining $n-4$ followers. □

Considering time-varying actions in the set of leaders, if the action in the followers is determined by the control law (5), they react only to positional errors, without anticipating the velocity of the leaders. The deformation tracking error can be reduced by means of a proportional–integral law, with a double-integral term to deal with accelerations. Integral terms in the following control law are directly adapted from [6], with provably global exponential convergence under leaders' motion. Considering $\mathcal{V}_f$ the set of vertices corresponding to follower agents in $\mathcal{G}$

$$
\begin{aligned}
{}^i u_i &= k_q \sum_{j\in\mathcal{N}_i} A_{ij}\,{}^i q_j + k_p\,{}^i p_j + k_r\,{}^i r_j \\
{}^i \dot{p}_j &= \sum_{j\in\mathcal{N}_i} A_{ij}\,{}^i q_j \\
{}^i \dot{r}_j &= \sum_{j\in\mathcal{N}_i} A_{ij}\,{}^i p_j, \forall i \in \mathcal{V}_f.
\end{aligned} \tag{29}
$$

Considering the following discrete-time control law:

$$
q(k+1) = q(k) + \tau u(k) \tag{30}
$$

where $q(k)$ and $u(k)$ are the state and the control input in iteration k and τ is the discretization factor. Then, the control input to the agent team during iteration $k \ge 1$ is given by

$$
\begin{aligned}
u(k) &= k_q\,A\,q(k) + k_p\,A\,p(k) + k_r\,A\,r(k) \\
p(k) &= p(k-1) + \tau\,q(k), \quad p(0) = 0_{2n} \\
r(k) &= r(k-1) + \tau\,p(k), \quad r(0) = 0_{2n}
\end{aligned} \tag{31}
$$

where $k_q > 0$, $k_p > 0$ and $k_v > 0$ are constant control gains. Detailed proof of the preservation of the closed-loop stability when including an integral term can be found in [6]. These parameters have been adjusted to ensure stability during the simulations and experiments below. As can be seen, in the control law (29), the integral terms ${}^i p_j$ and ${}^i r_j$ can be computed from the same relative measures ${}^i q_j$, keeping the control law distributed and independent of a reference frame.

III. Simulations

A series of simulations has been carried out, evaluating the performance of the method under different static and dynamic scenarios. The simulations were run on a PC with Intel Core i7-14700K 0x00040 3.40 GHz with 64 GB RAM, using MATLAB and Python, and the standard CVX [23] solver for optimizations. For the execution of the simulations, the discrete-time

This article has been accepted for inclusion in a future issue of this journal. Content is final as presented, with the exception of pagination.

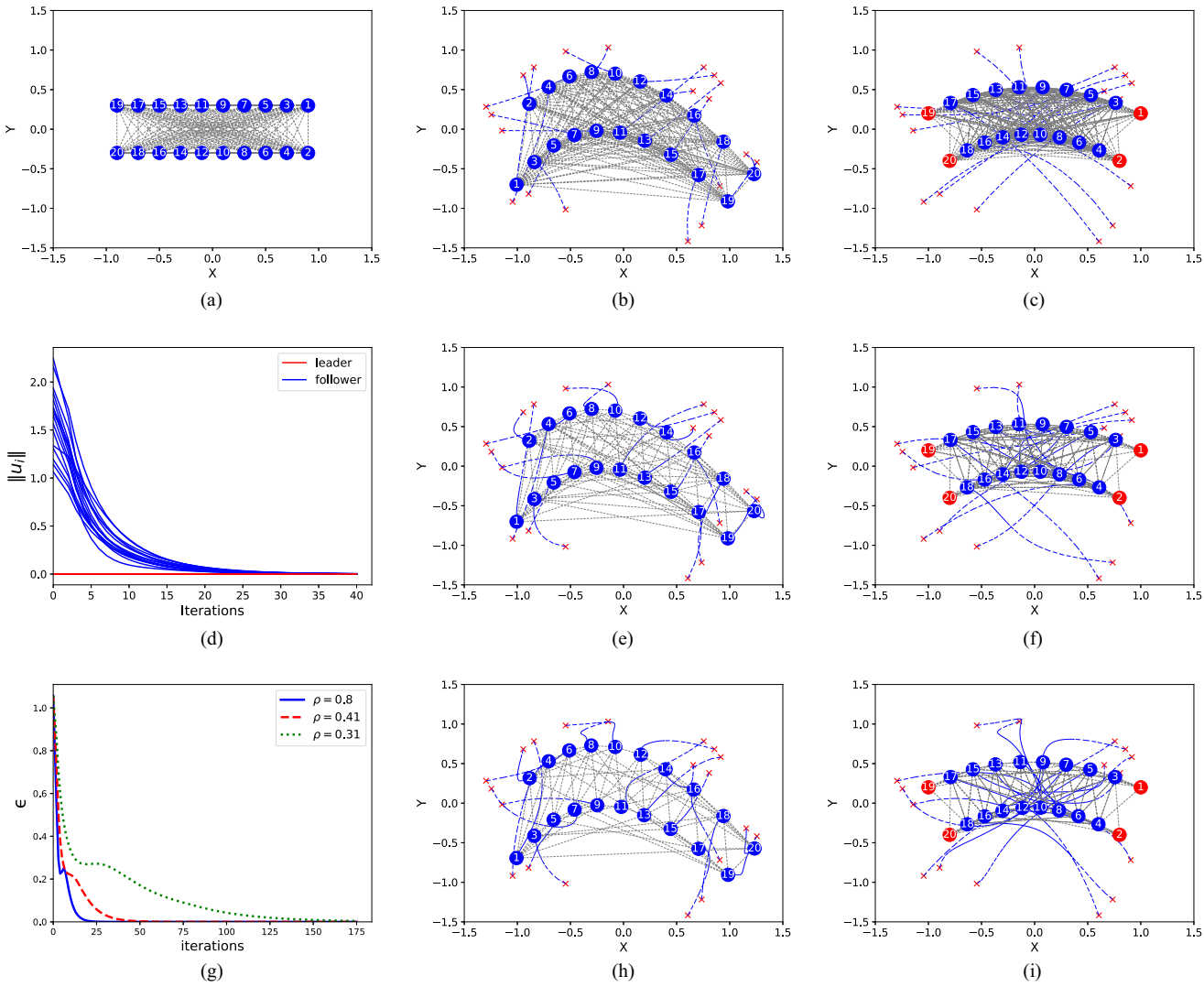


Fig. 2. Team of 20 agents moving in $\mathbb{R}^2$ towards quadratic transformations of the target configuration q^*. (a) Target configuration q^* with the dashed gray lines showing the connectivity between agents (blue dots) in a fully connected graph. (b), (e), and (h) Trajectories described by the agents towards $\mathcal{Q}(q^*)$ during the execution of the leaderless control (5) with link density $\rho = \{1, 0.5, 0.38\}$, and algebraic connectivity $\lambda_F = \{0.2, 0.064, 0.009\}$, respectively. The red crosses show the positions of the agents at the beginning, and the blue lines show the trajectories followed by the agents during the control. (c), (f), and (i) Trajectories described by the agents towards $\mathcal{Q}(q^*)$ during the execution of control (5) considering four static leaders, with link density $\rho = \{0.8, 0.41, 0.31\}$, and algebraic connectivity $\lambda_F = \{0.094, 0.047, 0.01\}$, respectively. The red dots correspond to the leader agents and the blue dots to the follower agents. (d) Evolution of agents' control input norm $\|u_i\|$, for the case in (c). (g) Evolution of the error ϵ (32) over iterations for the cases in (c), (f), and (h).

control (30) and the control laws (5), and (29) were used. Furthermore, to study the convergence to the quadratic deformation of q^*, the following interagent mean squared distance error is defined:

$$\epsilon = \frac{1}{n(n-1)} \sum_{i=1}^{n} \sum_{j \neq i} (\|{}^i q_j\| - \|{}^i q_j^{\infty}\|)^2 \tag{32}$$

being ${}^i q_j^{\infty}$ the relative state between agents in the formation obtained at the end of the control, precomputed as in (25).

In the first simulation, we will compare the performance of the proposed leaderless control (5) and the performance of the same control with four static leader agents. The convergence of the method has been simulated for different connectivity conditions, characterized by the algebraic connectivity λ_F (eigenvalue with minimum nonzero absolute real part value) and their link density ρ, computed as follows:

$$\rho = \frac{\text{card}(\mathcal{E})}{n(n-1)} \tag{33}$$

where $\text{card}(\mathcal{E})$ is the number of unidirectional connections. The offline calculation of the gain matrices was performed using MATLAB, with an estimated optimization time of around 6 s. Fig. 2(a) shows the team of 20 robots in the target formation q^*. Fig. 2(b) shows the result of the control without leaders, with every agent starting from a random position, depicted as a red cross, considering a fully connected graph and converging, describing the trajectories shown as blue dashed lines, to the final configuration. This resultant formation shows a resemblance to the ordering of agents in Fig. 2(a), but the distances between agents have changed, bending and rotating the formation until

This article has been accepted for inclusion in a future issue of this journal. Content is final as presented, with the exception of pagination.

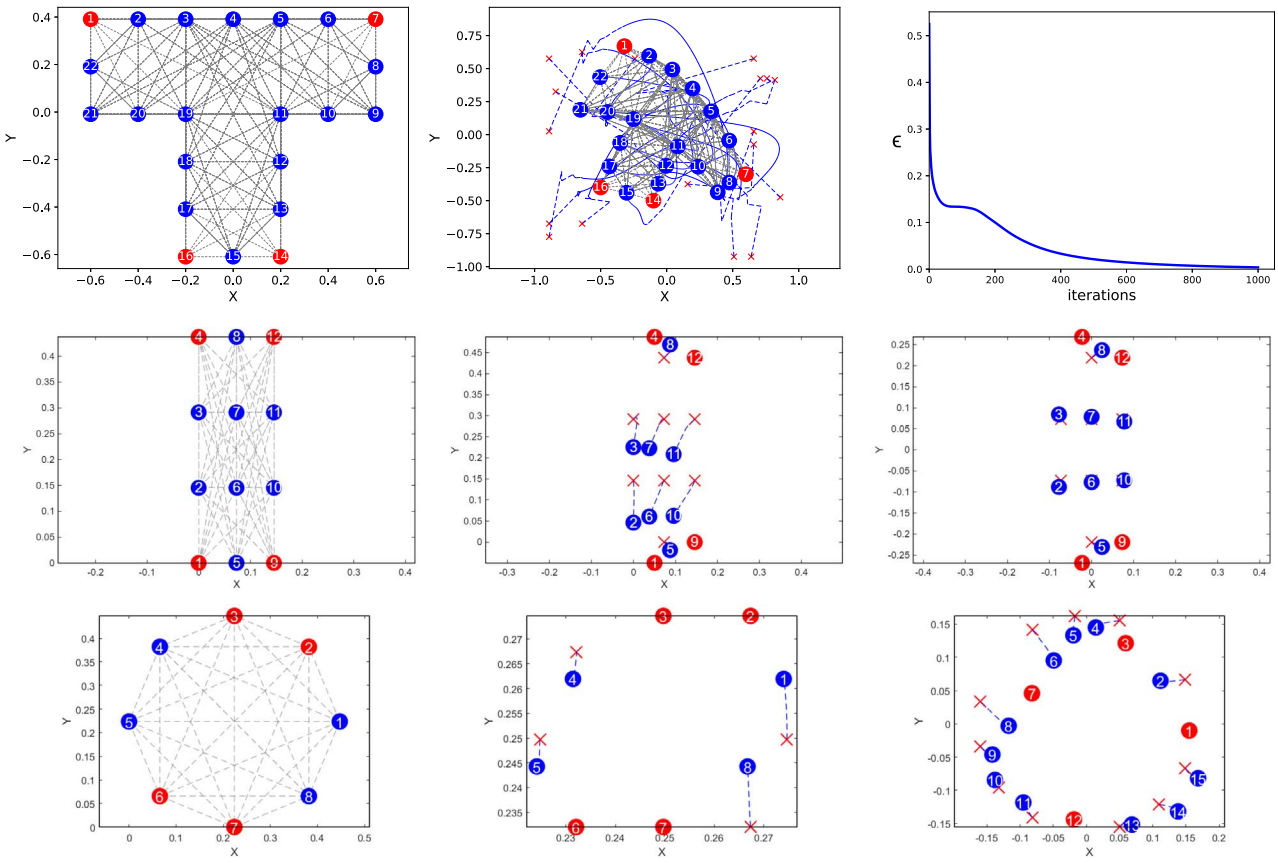


Fig. 3. First row: Team of 22 agents moving in $\mathbb{R}^2$ towards quadratic transformations of a T-shape q^*. Left: Target configuration q^* with the dashed gray lines showing the connectivity between agents. Center: Trajectories described by the agents towards $\mathcal{Q}(q^*)$ during the execution of control (5), considering agents 1, 7, 14, and 16 as static leaders. Right: Evolution of the error ϵ (32) over iterations. Second row: Team of 12 agents moving towards quadratic deformations of the grid-like target q^*. Left: Target configuration q^*. Center: Trajectories described by the agents towards $\mathcal{Q}(q^*)$, considering agents 1, 4, 9, and 12 as static leaders. Right: Trajectories described by the agents, with the same position of the leaders, but q^* is centered at the origin. Third row: Quadratic deformations of a circle. Left: reference circle configuration q^* for $n = 7$. Center: Trajectories described by the agents adapting to agents 2, 3, 6, and 7 as static leaders. Right: Trajectories described by the agents, being q^* a circle of 15 agents and agents 1, 3, 7, and 12 static leaders.

obtaining a deformation described by the following coefficient matrices in (2):

$$L_1 = \begin{bmatrix} -0.25 & -0.3 \\ 0.3 & -0.25 \end{bmatrix}, \; L_2 = \begin{bmatrix} 0 & 0.027 \\ -0.027 & 0 \end{bmatrix},$$
$$L_3 = \begin{bmatrix} 0.011 & 0.013 \\ -0.013 & 0.011 \end{bmatrix}, \; h = [1.3, -0.17]^\top. \tag{34}$$

Fig. 2(c) shows the control with agents 1, 2, 19, and 20 acting as leaders, with $\rho = 0.8$. The position of the leaders is static and corresponds to the desired configuration to which the followers must adapt. The initial position of the followers is the same as in Fig. 2(b). The fixed positions of the leaders impose a unique solution for the control convergence, regardless of the initial position of the followers, described by the following coefficient matrices in (2), which differ from those in (34):

$$L_1 = \begin{bmatrix} 0.174 & -0.127 \\ 0.127 & 0.174 \end{bmatrix}, \; L_2 = \begin{bmatrix} 0 & -0.015 \\ 0.015 & 0 \end{bmatrix},$$
$$L_3 = \begin{bmatrix} 0.01 & -0.006 \\ 0.006 & 0.01 \end{bmatrix}, \; h = [-0.8, -0.34]^\top. \tag{35}$$

In Fig. 2(c), we can see that the order of the collinear agents in Fig. 2(a) is preserved. Still, the rows of follower agents are quadratically deformed, increasing and decreasing their relative distance, to adapt to the position of the leaders. In this way, we can verify that four leaders are enough to establish restrictions on the deformation of q^* that would allow, for example, for maintaining the integrity of a deformable object during its transport.

On the other hand, Fig. 2(d) shows the evolution of the control input norm over iterations in the follower agents of the case depicted in Fig. 2(c). In this case, the computation of each iteration takes about 2 ms (without taking displacement into account). Both controls, with and without leaders, have been tested for different connectivity conditions. In Fig. 2(e) and (f), we have decreased ρ, decreasing also the values of λ_F, which in this case is less affected than in Fig. 2(c) by including leaders. Fig. 2(h) shows a case in which a small reduction in ρ causes a considerable decrease in λ_F. Last, Fig. 2(g) shows that connectivity affects the evolution of the mean squared distance error ϵ over the iterations, i.e., the control convergence, in cases 2(c), 2(f), and 2(i). It is shown how convergence speed

This article has been accepted for inclusion in a future issue of this journal. Content is final as presented, with the exception of pagination.

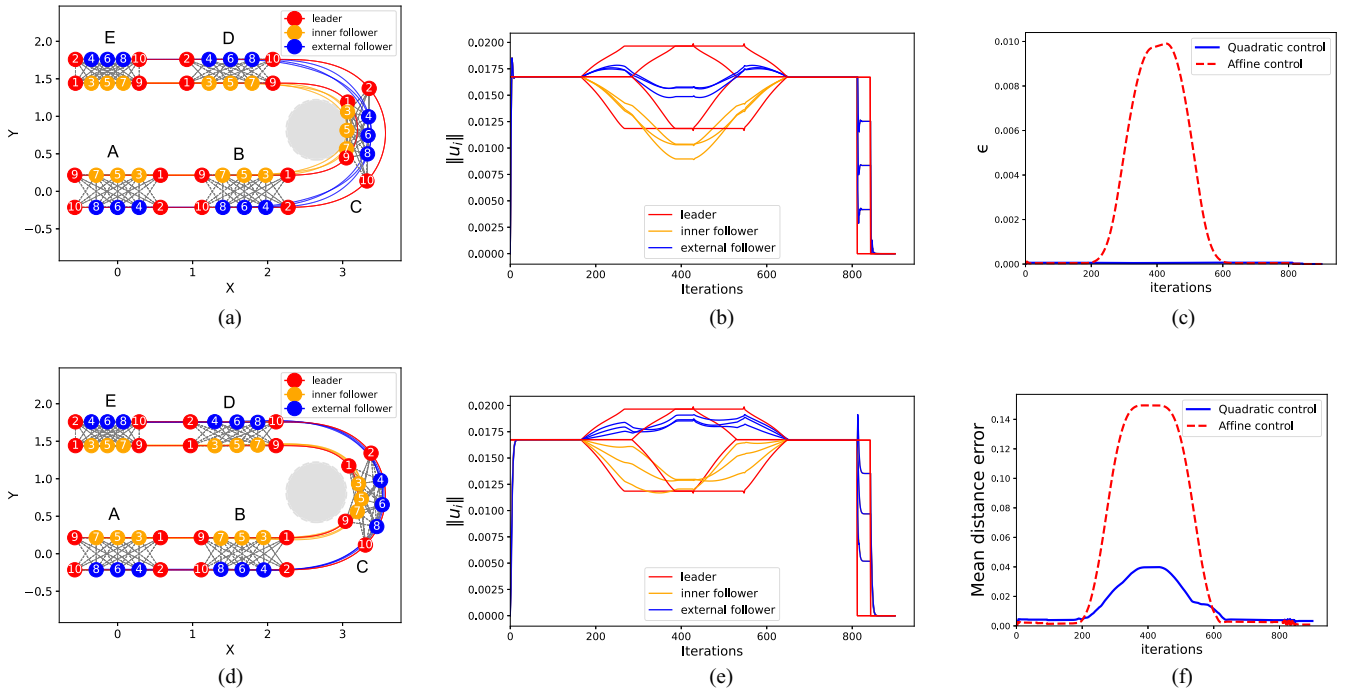


Fig. 4. Team of 10 agents moving along a predefined path to go around an obstacle in $\mathbb{R}^2$ under two different leader–follower control strategies. Red agents are leaders, blue agents are followers on the outer path, and orange agents are followers on the inner path. (a) Agents moving under an affine formation control law, describing different affine transformations of q^* (configuration A). (d) Agents moving under control law (29) describing different quadratic transformations in $\mathcal{Q}(q^*)$. (b) and (e) Evolution of agents' control input norm $\|u_i\|$, for the case in (a) and (d), respectively. (c) Comparison between the mean squared distance error ϵ of the quadratic-shape formation control and the mean squared distance error of the affine formation control, considering convergence to the affine image of q^*. (f) Comparison between the mean distance error of the position of follower agents to the trajectory of the leaders (red lines in Fig. 5) in each time instant, considering quadratic-shape formation control and affine formation control.

decreases as the connectivity of the graph is reduced. However, in the three cases, the error decreases asymptotically to 0, confirming that the configuration obtained at the end of the control belongs to the image of the solutions of $\mathcal{Q}(q^*)$.

To show the performance of the quadratic control (5) when faced with more complex configurations, the first row of images in Fig. 3 shows the case where it is applied to a T-shaped target configuration. As in the previous case, when the error ε converges asymptotically to 0, we find a formation of followers (blue dots) that adapts to the position of the leaders (red dots). This formation generates curves with those agents that are collinear, so that we can observe the T-shape bent to the right. The second row of Fig. 3 shows the case in which q^* is a grid-type formation. Achieving this type of formation would be of great complexity for methods such as [15] or [16], which are constrained to specific curve representations. A grid-type formation can be easily considered as a reference formation in our method and then be deformed quadratically using the leaders' positions. Regarding closed planar curves, our method cannot deform a collinear formation to high-frequency curves as those in [16]. Our method allows either to establish complex curves as reference formations q^* and deform them quadratically, or to obtain restricted quadratic deformations of simpler closed curves, as shown in the last row of Fig. 3. This feature can be useful for enclosing tasks with collision avoidance.

The scalability of the offline optimization (28) has been analyzed with additional optimization executions carried out for n between 4 and 50. We consider a cycle-type graph with four root agents so that $rank(A) = 2n - 8$ and random reference formations q^*. The execution time for each n has been obtained in five executions, and the mean values of the execution times are collected in Table I. They show that the optimization for n up to 50 agents can be carried out using standard equipment and solvers. Given the approximately exponential increase in the execution time, for a larger number of agents ($n > 50$), other practical scaling solutions may be needed. Examples of these solutions may be alternating direction methods [24] or methods considering specific topology structures [25].

TABLE I
EXECUTION TIME OF THE CVX-SDP [23] SOLVER WHEN COMPUTING OFFLINE GAIN MATRIX A, FOR $10 \leq n \leq 50$

Number of Agents (n)	10	20	30	40	50
CVX-SDP time (s)	0.45	5.75	38.14	151.95	459.70

The following simulation demonstrates the effectiveness of the control when the leader agents move along a specific curved path to round a static obstacle. The sequence shown in Fig. 4 is as follows: First, after moving in a straight line (configuration A to B), the leader agents describe a sharp curve to go around the obstacle (configuration C) and rotate the reference formation 180 degrees, while the distance between agents is reduced (configuration D). Then the rear leaders (agents 9 and 10) approach the front leaders so that at the end of the trajectory, we find a rotated and scaled version of the formation

This article has been accepted for inclusion in a future issue of this journal. Content is final as presented, with the exception of pagination.

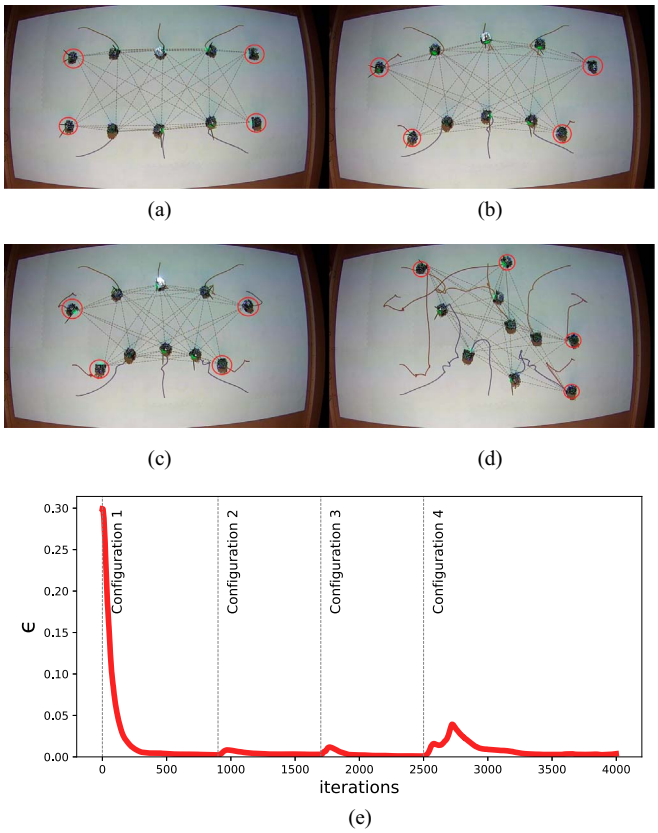


Fig. 5. Team of 10 agents under leader–follower strategy moving in $\mathbb{R}^2$ towards a series of quadratic transformations of the target configuration q^*. Leaders are marked with red circles. (a) Target configuration q^*. (b), (c), and (d) Configurations after convergence are quadratic transformations of q^* in $\mathcal{Q}(q^*)(2)$. (e) Evolution of the error ϵ (32) over iterations from the initial random configuration to the last target configuration 4.

(configuration E). Fig. 4(d) shows the trajectory followed by the agents under control in (30) and (31), with $k_q = 4$, $k_p = 3$, and $k_r = 3$. The resemblance between the trajectory of the leaders and the followers can be observed in the first segment (A and B). In the curved section (C), the formation bends in such a way that the following agents continue to describe a similar trajectory to that of the leader agents, avoiding collision with the obstacle. In the next segment (D), we can observe that the formation is able to scale until it reaches the target configuration (E). On the other hand, Fig. 4(a) shows this same trajectory under an affine formation control approach [6]. In this case, although the formation decreases its scale and gets the same target configuration (configurations D to E), the trajectory performed by the followers in the curve differs to a greater extent from that of the leaders, with respect to Fig. 4(d), resulting in the collision of followers 3 to 7 with the obstacle. Fig. 4(b) and (e) shows the evolution of the control input along the trajectory. They show a significant variation in control around the middle of the trajectory, corresponding to the agents' tracing of the curve. Comparing both plots, it can be observed that the control inputs in the quadratic control method are better adapted to the leader's control signals than in the affine control case, while dealing with the curved trajectory. In this case, the computation of the gain matrix took about 1.5 s, and the computation of the control inputs in each iteration took about 6 ms. Although the block-Laplacian matrices used have $\lambda_F = 1$ in the affine case and $\lambda_F = 0.35$ in the quadratic case, which indicates faster convergence in the affine case, this difference is not apparent in Fig. 4(c). This figure shows that ϵ is approximately 0 for both controls, but grows rapidly when moving along the curve in the affine case (with respect to the affine image of q^*). The difference in adaptability to the curve is also shown in Fig. 4(f), where the mean distance error of followers' trajectories with respect to the reference trajectory of the leaders is considerably bigger in the affine formation control.

This highlights the usefulness of quadratic control compared to other existing methods, which only consider affine transformations for formation control and maneuvering, such as [3], [6], [13], [14]. The proposed control not only maintains the ability to scale and rotate the formation, which is useful for crossing narrow corridors and avoiding obstacles, but also adds greater flexibility when tracing sharp curves or correcting orientation. Note that the variety of quadratic deformations obtainable is smaller than in [17], since the deformation space (2) eliminates anisotropic scales (shearing) from the possible deformations, which may be beneficial in transport tasks to maintain the integrity of the object. Compared to the formation control strategies in [15] and [16], our control allows for dynamically modifying the deformation, bending the formation to adjust to the curved path, while maintaining certain order among the agents. This feature facilitates avoiding collisions with static obstacles such as the one shown in Fig. 4, by adding appropriate constraints to the leaders. To handle more complex scenarios, including dynamic obstacles, the proposed formation controller can be integrated with a local reactive layer, such as a safety filter or barrier certificates, without compromising stability.

IV. Experiments

In this section, we extend the experiments to a real framework using Robotarium [26]. Their experimental setup is composed of unicycle-type robots. An approximation was used to adapt (5) into unicycle commands, projecting the single integrator system to a fixed distance from the unicycle. Thus, the following experiments validate the direct extension to this dynamics via an approximation, using the same gains computation as in the single-integrator case. Under more general dynamics, the guarantees presented in this article may not follow directly. Extending the proposed method beyond the single-integrator case is left for future work.

In these experiments, we continue with the leader–follower strategy proposed in Section II-E, and test both convergence in the face of different changes in leaders' positions, and the realization of curved trajectories maintaining formation. The first experiment is shown in Fig. 5, in which a group of 10 agents converges to a sequence of target configurations, using control (5), guided by the agents marked with a red circle. This figure also shows the agents' trajectories and the underlying connectivity graph, in the form of discontinuous gray lines. Fig. 5(e) shows the evolution of the interagent mean squared distance error ϵ defined in (32) throughout the experiment and

This article has been accepted for inclusion in a future issue of this journal. Content is final as presented, with the exception of pagination.

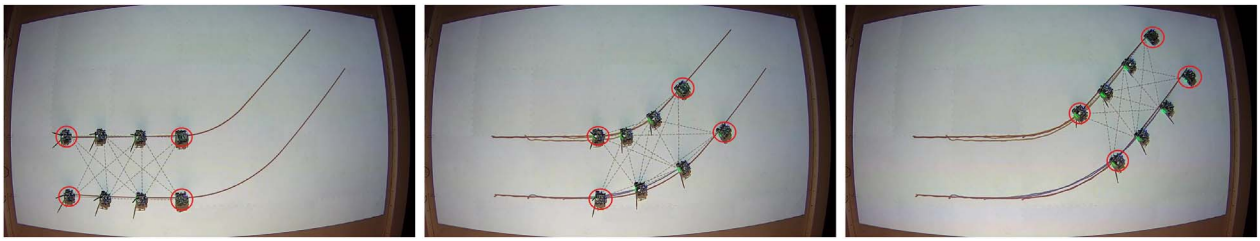


Fig. 6. Team of eight agents moving along a predefined path in $\mathbb{R}^2$ under the leader–follower quadratic-shape control strategies. Left and right: Initial and final states, respectively, where the agents are in roto-translated versions of the target formation q^*. Center: Intermediate state, where followers adapt to the curve followed by leaders by adopting a quadratic transformation in $\mathcal{Q}(q^*)$.

the iterations in which the leading agents begin to move to change the target formation. It shows that the most significant decrease in the error occurs when converging from the initial random positions to the first target configuration. Then, the agents are reconfigured into deformations of the same reference formation, resulting in less significant variations in error. The plot also shows that, for each of the configurations of the leaders, the followers converge to the corresponding configuration in $\mathcal{Q}(q^*)$ (2), with approximately zero error. The total execution time for this experiment was approximately 3 min.

In the following experiment, a team of eight agents follows a curved trajectory. Fig. 6 shows the curved trajectory, the trajectory followed by the agents, and their position in three different moments, as well as the underlying graph as in the previous experiment, with the leading agents marked with a red circle. The action of the followers is calculated according to the control law presented in (29), with $k_q = 2$, $k_p = 2$, and $k_r = 2$. At the initial state shown on the left side of Fig. 6, we can see the agents in the target configuration q^*, the same configuration shown on the right side of this figure at the final state, which has been rotated 45 degrees as a result of completing the curve. In the intermediate state shown in the middle of Fig. 6, the formation is traveling along the curve. As in the simulation in Fig. 4, quadratic-shape formation control allows the followers to adjust to the trajectory of the leaders while maintaining a certain degree of organization in the formation. The total execution time to complete the trajectory was approximately 1 min and 15 s.

Note that, although the Robotarium setup is indoor, the fact that the control is designed to work without a common coordinate frame facilitates its implementation in an outdoor environment. The difficulties of this extension are more related to sensing capabilities than to the controller design.

A supplementary video is included with the complete clips of all the experiments.

V. Conclusion

This article proposed a distributed control approach in 2-D that allows a multiagent formation to converge asymptotically to linear and quadratic deformations of a desired target formation. The presented method is applied under a leader–follower strategy to restrict the convergence and obtain specific configurations without knowledge of a global reference frame for the followers. This approach allows for making complex curves and traversing narrow corridors, improving flexibility when maneuvering compared to other methods like those based on affine transformations. The article provides theoretical analysis, simulations, and experiments, demonstrating the effectiveness of the method under different conditions. Future research may involve the extension to higher order agent dynamics, the reduction of tracking errors when following dynamic leaders, or the development of collision avoidance strategies to enhance adaptability to dynamic environments. Another interesting direction for future research is the study of distributed methods to compute the gain matrices, allowing variable interagent sensing topologies and improving scalability.

References

[1] D. Koung, O. Kermorgant, I. Fantoni, and L. Belouaer, "Cooperative multi-robot object transportation system based on hierarchical quadratic programming," *IEEE Robot. Automat. Lett.*, vol. 6, no. 4, pp. 6466–6472, Apr. 2021.

[2] K. Fathian, T. H. Summers, and N. R. Gans, "Robust distributed formation control of agents with higher-order dynamics," *IEEE Control Syst. Lett.*, vol. 2, no. 3, pp. 495–500, Mar. 2018.

[3] M. Aranda, R. Aragüés, and G. López-Nicolás, "Combined leaderless control of translational, shape-preserving, and affine multirobot formations," *IEEE Robot. Automat. Lett.*, vol. 8, no. 11, pp. 7567–7574, Nov. 2023.

[4] Z. Lin, L. Wang, Z. Han, and M. Fu, "A graph Laplacian approach to coordinate-free formation stabilization for directed networks," *IEEE Trans. Autom. Control*, vol. 61, no. 5, pp. 1269–1280, May 2015.

[5] K. Ze, W. Wang, K. Liu, and J. Lü, "Time-varying formation planning and distributed control for multiple UAVs in clutter environment," *IEEE Trans. Ind. Electron.*, vol. 71, no. 9, pp. 11305–11315, Sep. 2023.

[6] S. Zhao, "Affine formation maneuver control of multiagent systems," *IEEE Trans. Autom. Control*, vol. 63, no. 11, pp. 4140–4155, Nov. 2018.

[7] L. Wang, Z. Han, and Z. Lin, "Formation control of directed multi-agent networks based on complex Laplacian," in *Proc. IEEE Conf. Decision Control (CDC)*, pp. 5292–5297, 2012.

[8] K. Fathian, D. I. Rachinskii, T. H. Summers, M. W. Spong, and N. R. Gans, "Distributed formation control under arbitrarily changing topology," in *Proc. Am. Control Conf. (ACC)*, pp. 271–278, 2017.

[9] K. Fathian, S. Safaoui, T. H. Summers, and N. R. Gans, "Robust distributed planar formation control for higher order holonomic and nonholonomic agents," *IEEE Trans. Robot.*, vol. 37, no. 3, pp. 185–205, Mar. 2020.

[10] Z. Lin, W. Ding, G. Yan, C. Yu, and A. Giua, "Leader–follower formation via complex Laplacian," *Automatica*, vol. 49, no. 6, pp. 1900–1906, 2013.

[11] L. Chen, "Triangular angle rigidity for distributed localization in 2d," *Automatica*, vol. 143, 2022, Art. no. 110414.

[12] H. Pei, S. Chen, Q. Lai, and H. Yan, "Consensus tracking for heterogeneous interdependent group systems," *IEEE Trans. Cybern.*, vol. 50, no. 4, pp. 1752–1760, Apr. 2018.

[13] T. Wang et al., "Output affine formation maneuver control for heterogeneous multiagent systems with nonautonomous leaders," *IEEE Trans. Ind. Electron.*, vol. 72, no. 5, pp. 5376–5386, May 2025.

[14] P. Su, Z. Shi, J. Yu, X. Dong, Z. Ren, and D. Wang, "Distributed time-varying optimization-based protocols for affine formation maneuver,"

This article has been accepted for inclusion in a future issue of this journal. Content is final as presented, with the exception of pagination.

IEEE Trans. Ind. Electron., vol. 72, no. 8, pp. 8503–8511, Aug. 2025.

[15] M. Aranda, "Formation control on planar closed curves using Fourier descriptors," *IEEE Control Syst. Lett.*, vol. 7, no. 5, pp. 3391–3396, May 2023.

[16] B. Zhang, X. Shao, H. Zhi, L. Qiu, J. G. Romero, and D. Navarro-Alarcon, "Leader-follower formation control of perturbed nonholonomic agents along parametric curves with directed communication," *IEEE Robot. Automat. Lett.*, vol. 9, no. 10, pp. 8603–8610, Oct. 2024.

[17] R. Marcos-Saavedra, M. Aranda, and G. López-Nicolás, "Multirobot control with deformation modes for transport of deformable objects," *Int. J. Syst. Sci.*, vol. 24, no. 3, pp. 1–17, 2025.

[18] B. Yang, B. Lu, W. Chen, F. Zhong, and Y.-H. Liu, "Model-free 3-D shape control of deformable objects using novel features based on modal analysis," *IEEE Trans. Robot.*, vol. 39, no. 4, pp. 3134–3153, Apr. 2023.

[19] R. Herguedas, M. Aranda, G. López-Nicolás, C. Sagüés, and Y. Mezouar, "Double-integrator multirobot control with uncoupled dynamics for transport of deformable objects," *IEEE Robot. Automat. Lett.*, vol. 8, no. 11, pp. 7623–7630, Nov. 2023.

[20] J. Alonso-Mora, R. Knepper, R. Siegwart, and D. Rus, "Local motion planning for collaborative multi-robot manipulation of deformable objects," in *Proc. IEEE Int. Conf. Robot. Autom. (ICRA)*, pp. 5495–5502, 2015.

[21] Z. Lin, L. Wang, Z. Han, and M. Fu, "Distributed formation control of multi-agent systems using complex Laplacian," *IEEE Trans. Autom. Control*, vol. 59, no. 4, pp. 1765–1777, Apr. 2014.

[22] H. G. de Marina, "Distributed formation maneuver control by manipulating the complex Laplacian," *Automatica*, vol. 132, no. 4, 2021, Art. no. 109813.

[23] M. Grant and S. Boyd, "CVX: Matlab software for disciplined convex programming, version 2.1," Mar. 2014. [Online]. Available: https://cvxr.com/cvx

[24] P. C. Lusk, X. Cai, S. Wadhwania, A. Paris, K. Fathian, and J. P. How, "A distributed pipeline for scalable, deconflicted formation flying," *IEEE Robot. Automat. Lett.*, vol. 5, no. 4, pp. 5213–5220, Apr. 2020.

[25] A. Majumdar, G. Hall, and A. A. Ahmadi, "Recent scalability improvements for semidefinite programming with applications in machine learning, control, and robotics," *Annu. Rev. Control, Robot., Auton. Syst.*, vol. 3, no. 1, pp. 331–360, 2020.

[26] S. Wilson et al., "The Robotarium: Globally impactful opportunities, challenges, and lessons learned in remote-access, distributed control of multirobot systems," *IEEE Control Syst.*, vol. 40, no. 1, pp. 26–44, Jan. 2020.



Juan García-Lechuz received the B.Sc. degree in industrial engineering and the M.Sc. degree in robotics, graphics, and computer vision in 2021 and 2023, respectively, from the Universidad de Zaragoza, Zaragoza, Spain, where he is currently working toward the Ph.D. degree in systems engineering and computer science.

He worked as a master's student with the German Aerospace Centre (DLR), Wessling, Germany. He is a member of the Robotics, Perception and Real-Time Group at the Universidad de Zaragoza. His research interests include robotics manipulation, multirobot perception, and control.



Rosario Aragüés (Senior Member, IEEE) received the M.S. and Ph.D. degrees in system engineering and computer science from the Universidad de Zaragoza, Zaragoza, Spain, in 2008 and 2012, respectively.

From 2012 to 2013, she was a Postdoctoral Researcher at the Institut Pascal, CNRS, UMR 6602, Clermont-Ferrand, France. She is currently working as an Associate Professor with the Department of Computer Science and Systems Engineering, Universidad de Zaragoza. Her research interests include multirobot perception and control using distributed and decentralized strategies.



Gonzalo López-Nicolás (Senior Member, IEEE) received the Ph.D. degree in systems engineering and computer science from the Universidad de Zaragoza, Zaragoza, Spain, in 2008.

He is a Full Professor with the Department of Computer Science and Systems Engineering, Universidad de Zaragoza, where he is a member of the Robotics, Perception and Real-Time Group, and the Instituto de Investigación en Ingeniería de Aragón (I3A). His research interests include shape control, visual control, multirobot systems, and the application of computer vision techniques to robotics.